Published in final edited form as:
Science. 2010 January 29; 327(5965): 555–559. doi:10.1126/science.1182340.

Spontaneous and X-Ray Triggered Crystallization at Long Range in Self-Assembling Filament Networks

Honggang Cui[†], **Eugene T. Pashuck**[†], **Yuri S. Velichko**[†], **Steven J. Weigand**[‡], **Andrew G. Cheetham**[§], **Christina J. Newcomb**[†], and **Samuel I. Stupp**[*,†,§,‖,¶]
Department of Materials Science and Engineering, Department of Chemistry, and Department of Medicine, Northwestern University, 2220 Campus Drive, Evanston, Illinois 60208; DND-CAT Synchrotron Research Center, Northwestern University, APS/ANL 432-A004, 9700 S. Cass Avenue, Argonne, Illinois 60439; Institute for BioNanotechnology in Medicine, Northwestern University, Chicago, Illinois 60611

Abstract

We report here crystallization at long range in networks of like-charge supramolecular filaments mediated by repulsive forces. The crystallization is spontaneous beyond a given concentration of the molecules that form the filaments, but can be triggered by X-ray photons at lower concentrations. The crystalline domains formed by X-ray irradiation, with inter-filament separations of up to 320 angstroms, are stable for hours after the beam is turned off, and ions that screen charges on the filaments suppress ordering. We hypothesize that the stability of crystalline domains emerges from a balance of repulsive tensions linked to native or X-ray induced charges and the mechanical compressive entrapment of filaments within a network. Similar phenomena may occur naturally in the cytoskeleton of cells, and if induced externally in biological or artificial systems lead to possible biomedical and lithographic functions.

One-dimensional (1D) objects in solution such as carbon nanotubes (1), filamentous viruses (2), and rigid molecules (3) can spontaneously form orientationally ordered domains or networks as a result of their shape. This well known excluded volume effect is useful in the design of devices, liquid crystals, high strength materials, hydrogels, and other functional structures. In biological systems, the bundling, orientation, and mechanical networking of 1D cytoskeleton components such as filamentous actin and microtubules mediate cellular events such as mitosis, protein transport and signal transduction (4–9). There is also rapidly growing interest in the development of artificial extracellular matrices for cell signaling based on self-assembling fibril networks (10–12). In this area it is important to learn more about structural features in 3D networks and their role in mechanical properties and bioactivity (13).

Small angle X-ray scattering (SAXS), which employs selective detection of elastically scattered X-rays, has advanced to be one of the most powerful methods to characterize the structure of materials at the nanoscale, providing information on the size, shape, and symmetry of their internal domains(14, 15). The technique is in fact extremely useful to study structures with the length scales of 3D networks formed by nanoscale filaments (4). At the same time, the high brilliance of X-ray beams in third generation synchrotron sources

[*]Corresponding author: s-stupp@northwestern.edu.
[†]Department of Materials Science and Engineering
[‡]DND-CAT Synchrotron Research Center
[§]Institute for BioNanotechnology in Medicine
[‖]Department of Chemistry
[¶]Department of Medicine

can induce irreversible chemical changes in organic molecules and consequently on their three dimensional structures (16–18). The typical mechanisms involve ejection of energetic electrons from molecules via the well-known photoelectric, Compton, and Auger effects, resulting in the formation of free radicals, charged molecules, as well as chemical reactions (19–23). These phenomena can also be useful in lithographic techniques (24), photoelectrochemistry (25), polymerization (26), cancer therapies (27), mutations for biological research (28), and studies on RNA conformation dynamics (29).

We report here the spontaneous and X-ray triggered crystallization of supramolecular filaments within 3D networks at surprisingly large distances (up to 320Å). The filaments described here are formed by self-assembly in water of a synthetic molecule containing the short peptide sequence A_6E_3 covalently grafted to an alkyl chain of 16 carbons (Fig. S1). A representative cryogenic transmission electron microscopy (cryo-TEM) image is shown in Fig. 1A, revealing cylindrical nanofibers measuring ~102 Å in diameter corresponding to twice the fully extended length of the molecules. The length of the filaments can not be directly obtained from cryo-TEM but it is estimated to be on the scale of tens of micrometers. The combined effect of intermolecular hydrogen bonding among the peptide segments and hydrophobic collapse of hydrocarbon tails in these molecules leads to formation of the 1D nanostructures in dilute solution (10, 30). We observed that the SAXS profiles of 0.5 wt % solutions dramatically changed upon continuous X-ray exposure. Fig. 1B displays 50 sequential SAXS profiles of the same spot with an exposure time of four seconds each, plotted on a double-logarithmic scale. The first spectrum (red) shows a typical scattering profile of cylindrical objects in solution, as suggested by the −1 slope in the low q region and a diffuse form factor peak around 0.1 $Å^{-1}$ (31) (Fig. S3). Successive irradiation on the same spot yielded a series of Bragg peaks. The relative positions of the peaks follow the q/q^* ratios of 1: $\sqrt{3}$: $\sqrt{4}$: $\sqrt{7}$: $\sqrt{9}$: $\sqrt{12}$ (where q^* is the principal peak position), characteristic of a highly ordered two-dimensional hexagonal lattice (*p6mm*). The development of scattering profiles is characterized by the emergence and continued increase in intensity of the principal Bragg peak, as well as the appearance of additional peaks at higher *q* values. Fig. 1C shows the 2D scattering patterns of the first and the last exposures, clearly revealing the disorder-to-order transition. The low volume fraction of filaments (0.5 wt %) indicates that these hexagonally packed 1D objects must exist as bundles. We measured the final values of full width at half maximum and used the Scherrer equation to estimate a bundle size. The calculation yields a value of approximately 1 micrometer, however, given the size regime the absolute value obtained from the Scherrer equation is of questionable accuracy. The Debye-Sherrer ring-like pattern after X-ray exposure is typical of scattering from a powder sample, implying that these hexagonal crystalline bundles are randomly distributed in solution (Fig. 1D).

We found that this X-ray-triggered structural rearrangement only occurs at relatively low concentrations. Fig. 2A shows a similar disorder-to-order transition observed at 1 wt % upon continued X-ray irradiation. However, at higher concentrations (2 wt % and higher), the Bragg peaks are observed without the need for continuous X-ray irradiation (Figs. 2B and 2C). The hexagonally stacked filaments at 2 wt % and 5 wt % are stable to X-ray exposure and their corresponding Bragg peaks do not change considerably with accumulated exposure time. These observations suggest that hexagonal stacking of filaments at higher concentration is a spontaneous process and not associated with X-ray irradiation. The X-ray profiles corresponding to the last exposure for various concentrations have been replotted in Fig. 2D. Five to seven Bragg peaks are registered in each scattering profile and have the expected relative ratios of hexagonal structures. The Bragg peak positions shift smoothly to higher values of *q* with an increase in peptide concentration in both spontaneous and X-ray triggered hexagonal structures. This corresponds to a decrease in inter-filament separation as

the concentration rises (Fig. 2E), and suggests the spontaneous and X-ray triggered hexagonal structures emerge through similar mechanisms.

To determine if X-ray beam heating could contribute to this structural disorder-to-order transition, we studied the 1 wt % A_6E_3 solution at 25°C and 40°C. We found that Bragg peaks did not appear after the first four-second exposure at 40°C, and the overall scattering profiles undergo a very similar transition as those obtained at 25°C (Fig. S2). Fig. 2F shows the relative change in the q^* peak intensity plotted with respect to the exposure time, suggesting no obvious difference between 25°C and 40°C. In addition, Caffrey and co-workers reported only a 0.16°C temperature rise as a result of continuous X-ray exposure of Milli-Q water (20). Since beam heating results typically in only a small temperature change due to the rapid dissipation of heat into the local environment, one does not expect this thermal effect alone to contribute to the observed structural transition (Fig. S4).

Another important observation was the reversal of the X-ray triggered crystalline structures to a disordered state after removal of the beam. Macroscopically, the 1 wt % solution in the capillary was clear before X-ray irradiation (Fig. 3A). Following X-ray exposure (accumulated 200 seconds), the spot of interest became opaque (position 1 in Fig. 3A). This appearance of turbidity is indicative of a transition between two states with different structural order, possibly due to scattering by crystalline filament domains. After removal of the X-ray beam, the solution gradually became clear and completely lost its opacity within approximately 40 minutes. This reversible opacity was further investigated with scattering experiments. Fig. 3B shows the transition from disordered filaments (the first four-second exposure) to the hexagonally ordered bundles (the last four-second exposure). Two hours after removing the X-ray beam, scattering profiles were collected on the same location. We found that all peaks corresponding to hexagonal filament stacking vanished, thus suggesting the loss of positional order (Fig. 3C). Restarting X-ray irradiation causes the reappearance of Bragg scattering peaks. This reversibility is also observed when adjacent regions to the originally irradiated spot are exposed to X-rays. This experiment suggests that reversibility is not caused by simple diffusion of chemically unmodified material into the originally irradiated spot. In fact, analytical HPLC and mass spectrometry of samples after a large X-ray dose confirmed that chemical damage is not involved in the observed reversible phenomenon (supporting information S8).

In order to gain more insight into the observed X-ray induced phenomenon, we studied the effects of beam flux and photon energy. We found that a longer exposure time was required to induce this disorder-order transition when the X-ray beam was gradually attenuated (Fig. 3E). However, in order to induce filament ordering, a larger irradiation dose was needed when samples were exposed to X-rays at a lower dose rate (smaller beam flux) (Fig. 3F). Eventually, at a beam attenuation of 0.012, the Bragg peaks corresponding to the hexagonally ordered filaments did not appear even with an accumulated 1,120 second exposure (Fig. 3G), and a total dose approximately twice as large as that needed to induce the filament ordering with a non-attenuated beam (4.39×10^4 Gy) (Fig. S5). Radiation damage by X-rays has been reported as more severe when samples are irradiated with a fixed accumulated dose but at a lower dose rate (the inverse dose-rate effect (22)). Therefore, in this context, if chemical damage did occur, and the resulting products were responsible for filament ordering, the same accumulated dose at a lower dose rate should have enhanced the effect. These dose rate-dependent experiments again support that a reversible process is involved. We also found that filament ordering can be induced using X-ray photons with a lower energy (9 keV vs. 15 keV) (Fig. 3D), suggesting much weaker beams can be used to promote ordering given that lower energy photons have a higher mass-energy absorption coefficient.

A striking feature of the observed hexagonal crystalline structures formed spontaneously or triggered by X-rays is the large *d*-spacing among filaments (Fig. 2E). The center-to-center spacing is as large as 320 Å for 0.5 wt % solutions (X-ray triggered) (Fig. 2F). Given the 102 Å diameter of the filaments, the wall-to-wall distances measured range between 218 Å and 90 Å for concentrations of 0.5 wt % and 5 wt %, respectively. These distances are surprisingly large compared to others reported in the literature among cytoskeleton filaments and DNA strands (4, 32, 33). In these systems the distances measured are in the range of 30 to 55 Å and always in the presence of multivalent counterions which should introduce attractive forces among like-charge objects. The multivalency of added counterions, not added in our systems, is critical to induce positional ordering through attractive forces in these biomolecular systems. In one example, Safinya and coworkers have observed both hexagonal and necklace bundles in microtubule filaments after adding multivalent counterions (4). The structures are viewed as resulting from the balance among electrostatic repulsion and attraction as well as hydration forces (repulsive) and van der Waals interactions. Since multivalent counterions are not added in our systems, attractive electrostatic interactions cannot be considered as offsetting repulsive forces among the filaments. At the same time, van der Waals forces are not expected to stabilize repulsions at the inter-filament distances of hundreds of angstroms observed here. We therefore hypothesize that crystalline stacking of filaments emerges from the minimization of repulsive electrostatic interactions balanced by other attractive forces associated with network structures.

To understand the observed disorder-to-order transition, it is useful to consider first the origin of bundle formation. Our insight is that bundle formation from filaments with very high aspect ratios must occur during their supramolecular growth. This is suggested because these extremely long and networked filaments are unlikely to reorganize into bundles on short time scales once they are formed. TEM reveals the coexistence of very short and very long filaments at the very early stages of self-assembly (see Fig. 4E). Based on this observation, we hypothesize that long filaments formed at early stages create a stable network that templates the formation of bundles as growth of short filaments continues. As depicted in Fig. 4A, this “templating” effect can be envisioned as further parallel growth of filaments around the originally formed network. At the moment the precursor network is formed, topological constraints due to interlocking of filaments would limit their mobility within a tube-like channel around each of them (Fig. 4Ai). Therefore, the dimension of the channel would actually limit the size of the bundles formed. Long filaments can only move freely within their own channels, while shorter filaments can move in and out without any restrictions. Newly formed long filaments will be preferentially confined within one of these channels due to their local rigidity and high aspect ratio, as well as the long-range electrostatic repulsions among the filaments (Fig. 4Aii). We assume that the growth of spatially correlated filaments in the limited space provides the foundation for the observed filament stacking. At 1 wt % or lower, subsequent filament growth within the space-confined channels eventually results in formation of loosely packed filament bundles that lack positional order (Fig. 4Aiii). The increasing number of filaments within the bundles as concentration is increased can be in fact readily observed by cryo-TEM (Fig. 4B-D). We suggest that beyond a critical concentration, electrostatic repulsions within bundles combined with our hypothesized network forces lead to hexagonal ordering of filaments (Fig. 4Aiv). The interactions between these like-charge filaments depend not only on the inter-filament distance and their mutual orientation, but also on the three-dimensional structure of the electric double layers arising from condensed and mobile ions. The theoretical analysis of electrostatic interactions within the bundles would require solving Poisson’s equation with boundary conditions for a system of parallel filaments,

$$\nabla \cdot (\overleftrightarrow{\varepsilon}\vec{E}(\vec{r})+\vec{P}(\vec{r}))=\rho(\vec{r})$$

where $\varepsilon\leftrightarrow$ is the dielectric permittivity tensor, $\vec{E}(\vec{r})$ is the electric field that determines the strength of electrostatic interactions, $P\rightarrow(\vec{r})$ describes the polarization of dielectric interfaces, and $\rho(\vec{r})$ is the free charge density. For systems with high surface charge in the presence of dielectric interfaces, charge correlations and interface polarization lead to intractable mathematical problems (34), clearly beyond the scope of this work.

The crystallization at long range driven by 200 second exposure to X-rays supports strongly the presence of bundles even in very dilute networks. The gradual rise in intensity of the principal Bragg peak suggests that more crystalline bundles are being formed upon continuous X-ray exposure. Also, based on the Scherrer equation, the observed decrease with further exposure in full width at half maximum of this peak suggests that crystalline bundles are increasing in size. During this period of time, we do not expect reorganization of the extremely long filaments across a large volume and therefore crystallization must be occurring locally within the bundles. At the same time, the observed reversibility between the disordered and hexagonally ordered states at low concentrations suggests that inter-filament forces must be changing as a result of X-ray exposure. X-ray irradiation is likely to increase the charge density on filament surfaces (22, 23, 35), thus altering the balance of forces within the bundles of the dilute network. This new balance of forces induced by X-rays must resemble that prevailing in the spontaneous crystallization of bundles at high concentration. If electrostatic repulsive forces among the filaments are mediating crystallization at long range, they must be acting in concert with a balancing attractive force. We hypothesize that this attractive force could be rooted in the structural integrity of the entire network. The spatial confinement imposed by neighboring bundles in the network acts effectively as an “attractive” force balancing repulsion among the like-charge filaments. The stability of these networks containing crystalline bundles of like-charge filaments may therefore originate in tension linked to repulsive forces within each bundle balanced by compression forces associated with the network. In this context, it is interesting that crystallization within the bundles provides a mechanism to minimize the local tension from repulsive forces. This balance is reminiscent of that existing in self-stabilizing tensegrity networks (8, 9).

We carried out experiments to demonstrate the involvement of repulsive electrostatic forces in crystallization at long range within the filament bundles. These experiments involved adding NaCl and $CaCl_2$ to 1 wt % solutions in order to screen electrostatic forces among like-charge filaments. We found that the primary Bragg peak developed more slowly during continuous X-ray irradiation as the amount of NaCl was increased (see Fig. 4F and Fig. S4). At a concentration of 50 mM NaCl or higher, the X-ray induced crystallization was not observed at all even after an accumulated exposure time of 120 seconds. Fig. 4G shows 50 sequential scattering profiles of 1 wt % solution in the presence of 50 mM NaCl. When the divalent salt $CaCl_2$ was used even in concentrations as low as 5mM the crystalline structures were never observed. We also found that addition of 5mM NaOH can promote filament ordering at 1 wt % without exposure of samples to X-ray irradiation. NaOH can increase charge density on the acidic nanofiber surfaces by deprotonating COOH groups in glutamic residues (Fig. S7). These observations support our hypothesis that electrostatic repulsions mediate crystallization of the filaments at long range. Our experiments also suggest that the observed reversible X-ray triggered crystallization results from increasing charge density on filament surfaces.

To investigate further if this charge density increase is associated with permanent chemical modifications by the X-ray photons, we carried out chemical analysis on a sample irradiated with a large dose of X-rays. Even when approximately 60% of the total volume of a sample was irradiated with a dose 44 times higher than is needed to generate filament ordering, chemical changes were still not observed using a UV-vis detector. Only mass spectrometry detection could reveal a very small amount of chemically modified byproducts (Supporting information S8). It is well known that, in acidic, air-saturated aqueous solutions, the dominant species of water radiolysis are hydroxyl radicals (•*OH*) and hydrated electrons (e^{-}_{aq}); both could potentially react with peptide backbones and side chains in various ways and yield products such as ammonia, keto acids, aldehydes and other peptide derivatives (23). Among these products, α-hydroxyl carboxylic acids and α-keto acids could potentially contribute to an increase in charge density due to their slightly lower pKa values. Interestingly, detailed chemical analysis using mass spectrometry indicate that hydroxylation products are only associated with the alkyl tails and the first alanine residue adjacent to the tail. Our data also show that the very small amount of α-hydroxylation occurring in the glutamic acid residues results in main-chain cleavage and formation of amide-terminated products (supporting information S8). We conclude that none of these species contribute significantly, if at all, to the increase in charge density on the surfaces of filaments. Considering the fact that oxygen plays a very important role in mediating this irreversible chemical reaction to generate the α-hydroxylation products, we performed experiments in an oxygen-free solution and found that X-ray irradiation was still able to induce the ordering of filaments (Fig. S10). This experiment provides additional evidence that permanent chemical damage mediated by soluble oxygen in water is not necessary to facilitate filament ordering. In addition, we have observed filament ordering in other peptide molecules with different sequences, for example, VVAAEEGGREDKETV and VVAAEEGGTKREEVD (Fig. S11), further suggesting that the mechanism of charge density increase on filament surfaces is not specifically linked to glutamic acid residues but is instead a more general phenomenon.

Based on evidence described above, we propose that the main mechanism responsible for an increase in charge density on peptide nanofiber surfaces is linked to the reversible ionization of the COOH groups by X-ray irradiation. Since we obtained direct experimental evidence for filament ordering as a result of carboxyl ionization with strong base, we speculate that the enhanced electrostatic repulsions among filaments leading to crystallization arise from deprotonation of COOH directly caused by X-ray irradiation (supporting information S9). Hydroxide ions produced by water radiolysis may also contribute to the enhanced ionization of carboxyl groups. Because of the high packing density of COOH on the surfaces of these extremely long filaments, a very small percentage of ionized COOH groups could potentially lead to a considerable increase in electrostatic repulsion among filaments, and thus produce the observed ordering. It is also possible that hydrated electrons produced by water radiolysis can contribute to electrostatic repulsion through their addition to the C=O bonds (23). The charged species can return to their original structures through a previously proposed reconstitution mechanism (23) (Supporting information S9).

We have reported crystallization mediated by repulsive forces of high aspect ratio like-charge filaments within a network environment. We believe arrangement of the filaments into aligned bundles trapped within a network is necessary for the observed crystallization, and can be templated during growth of the very long filaments by self-assembly. The supramolecular nature and role of electrostatics in systems studied here create a connection to cytoskeleton filaments where similar crystalline bundles embedded in networks could occur naturally or be artificially created by externally regulated charge density. The observed X-ray triggered and reversible crystallization of the filaments at very low concentrations offers opportunities to create the ordered structures without specific design of

molecules with photon-sensitive chemistry, or to study 1D object dynamics vs. charge given the temporal stability of the transient crystals. At the same time, the ability of X-ray photons to easily penetrate tissues could lead to biomedical applications based on network crystallization within cells or therapeutic hydrogels. Another possibility is to explore filament crystallization through charge in lithography of soft matter.

Supplementary Material

Refer to Web version on PubMed Central for supplementary material.

Acknowledgments

This work was supported by the U.S. Department of Energy (Grant No. DE-FG02-00ER45810), by the National Science Foundation (MRSEC at Northwestern University Grant No. NSF DMR-0520513) and by the National Institutes of Health (Grants 5 R01 DE015920-04 and 5 U54 CA119341-04). The small-angle X-ray scattering (SAXS) experiments were performed at the DuPont-Northwestern-Dow Collaborative Access Team (DND-CAT) located at Sector 5 of the Advanced Photon Source (APS). DND-CAT is supported by E.I. DuPont de Nemours & Co., The Dow Chemical Company and the State of Illinois. Use of the APS was supported by the U. S. Department of Energy, Office of Science, Office of Basic Energy Sciences, under Contract No. DE-AC02-06CH11357. The authors are also grateful to Biological Imaging Facility (BIF) at Northwestern for the use of TEM equipment.

References

1. Song WH, Kinloch IA, Windle AH. Science. Nov.2003 302:1363. [PubMed: 14631032]
2. Lee SW, Mao CB, Flynn CE, Belcher AM. Science. May.2002 296:892. [PubMed: 11988570]
3. Nakata M, et al. Science. Nov.2007 318:1276. [PubMed: 18033877]
4. Needleman DJ, et al. Proc Natl Acad Sci U S A. Nov.2004 101:16099. [PubMed: 15534220]
5. Pelletier O, et al. Phys Rev Lett. Oct.2003 91:4.
6. Gardel ML, et al. Science. May.2004 304:1301. [PubMed: 15166374]
7. Bathe M, Heussinger C, Claessens M, Bausch AR, Frey E. Biophysical Journal. Apr.2008 94:2955. [PubMed: 18055529]
8. Ingber DE. Annu Rev Physiol. 1997; 59:575. [PubMed: 9074778]
9. Wang N, Butler JP, Ingber DE. Science. May.1993 260:1124. [PubMed: 7684161]
10. Hartgerink JD, Beniash E, Stupp SI. Science. Nov.2001 294:1684. [PubMed: 11721046]
11. Aggeli A, Bell M, Boden N, Carrick LM, Strong AE. Angew Chem-Int Edit. 2003; 42:5603.
12. Haines-Butterick L, et al. Proc Natl Acad Sci U S A. May.2007 104:7791. [PubMed: 17470802]
13. Engler AJ, Sen S, Sweeney HL, Discher DE. Cell. Aug.2006 126:677. [PubMed: 16923388]
14. Chu B, Hsiao BS. Chemical Reviews. Jun.2001 101:1727. [PubMed: 11709997]
15. Lipfert J, Doniach S. Annu Rev Biophys Biomolec Struct. 2007; 36:307.
16. Cherezov V, Riedl KM, Caffrey M. J Synchrot Radiat. Dec.2001 9:333.
17. Ravelli RBG, McSweeney SM. Struct Fold Des. Mar.2000 8:315.
18. Teng TY, Moffat K. J Synchrot Radiat. Sep.2000 7:313.
19. Nave C. Radiation Physics and Chemistry. Mar.1995 45:483.
20. Cheng AC, Caffrey M. Biophysical Journal. May.1996 70:2212. [PubMed: 9172745]
21. Weik M, et al. Proc Natl Acad Sci U S A. Jan.2000 97:623. [PubMed: 10639129]
22. Stark G. Biochimica Et Biophysica Acta. Jul.1991 1071:103. [PubMed: 1854791]
23. Garrison WM. Chemical Reviews. Apr.1987 87:381.
24. Ehrfeld W, Lehr H. Radiation Physics and Chemistry. Mar.1995 45:349.
25. Ma Q, Divan R, Mancini DC, Keanet DT. J Phys Chem A. May.2008 112:4568.
26. Collinson E, Dainton FS, McNaughton GS. Transactions of the Faraday Society. 1957; 53:476.
27. Eisbruch A. Nat Clin Pract Oncol. Jan.2005 2:34. [PubMed: 16264854]
28. Thomas JW, LaMantia C, Magnuson T. Proc Natl Acad Sci U S A. 1998; 95:1114. [PubMed: 9448294]

29. Sclavi B, Sullivan M, Chance MR, Brenowitz M, Woodson SA. Science. Mar.1998 279:1940. [PubMed: 9506944]
30. Velichko YS, Stupp SI, de la Cruz MO. J Phys Chem B. Feb.2008 112:2326. [PubMed: 18251531]
31. Pizzey CL, et al. J Chem Phys. Sep.2008 129:8.
32. Bloomfield VA. Biopolymers. 1997; 44:269. [PubMed: 9591479]
33. Pelta J, Durand D, Doucet J, Livolant F. Biophysical Journal. Jul.1996 71:48. [PubMed: 8804588]
34. Parsegian, VA.; Van der Waals. Cambridge University Press. 2005. p. 239
35. Collet E, et al. Science. Apr.2003 300:612. [PubMed: 12714737]

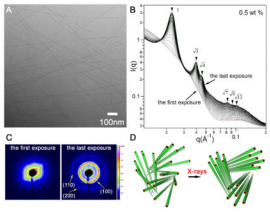

Figure 1.

X-ray irradiation triggered crystallization of self-assembling filaments at 0.5 wt % aqueous solutions of a peptide amphiphile. **(A)** Representative cryo-TEM image of filaments formed in 0.5 wt % solutions of peptide amphiphile; **(B)** a series of 50 consecutive scattering profiles of 0.5 wt % solutions obtained from the same sample area with four second exposure each (dose rate: 4806 Gy/second). The measurements were performed at room temperature with a monochromic X-rays at 15keV, and the typical incident X-ray flux on the sample was ~1×10^{12} photons/s with a 0.2×0.3 mm^2 collimator (samples were placed inside quartz capillaries of a diameter of 2 mm). The first and the last spectra are colored red and green, respectively; **(C)** 2D scattering patterns corresponding to the first and last exposures in **B; (D)** schematic representation of X-ray triggered organization of peptide filaments from a disordered state to a hexagonally ordered state.

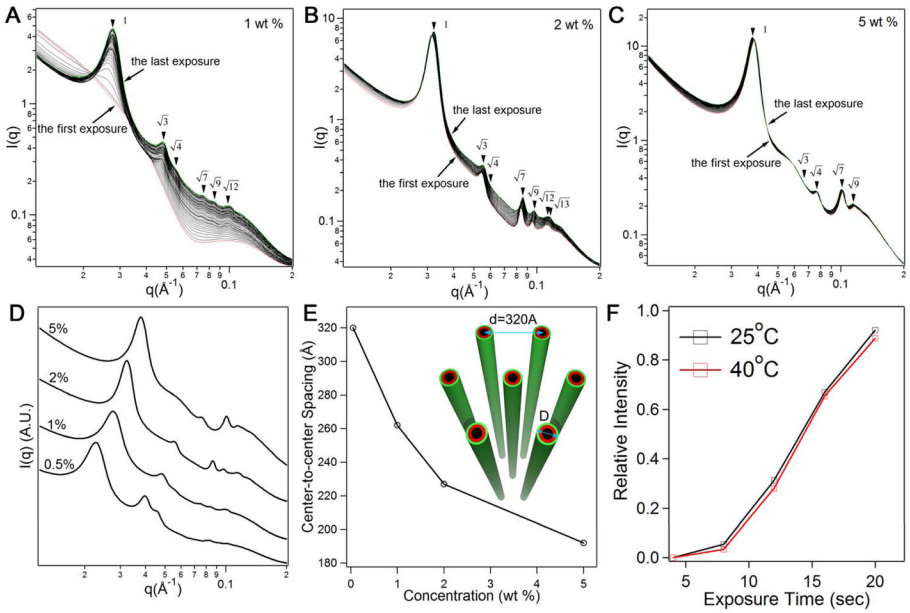

Figure 2.

Concentration dependence and temperature effect of X-ray triggered filament crystallization. **(A)** 50 consecutive scattering profiles from 1 wt % aqueous solutions (exposure time: 4 seconds); (**B**) 30 consecutive scattering profiles from 2 wt % solutions (exposure time: 2 seconds), and 5 wt % solutions (exposure time: 1 second) (**C**) (the dose rate for the experiments in (A–C) was 4806 Gy/second). The first and the last profiles in **A**, **B**, and **C** are colored red and green, respectively; **(D)** a replot of X-ray scans corresponding to the last exposure at concentrations of 0.5 wt %, 1 wt %, 2 wt % and 5 wt %; **(E)** a plot of center-to-center spacings among filaments as a function of peptide amphiphile concentration (the inset shows a schematic representation of the largest spacing observed among filaments in 0.5 wt % solutions); (**F**) effect of temperature on X-ray triggered ordering of the filaments in a 1 wt % solution (the relative intensity is given by $(I_n - I_4)/I_4$ where n denotes the accumulated exposure time and I_4 is the intensity value at the location of the principal Bragg peak in the first scattering profile obtained after X-ray irradiation).

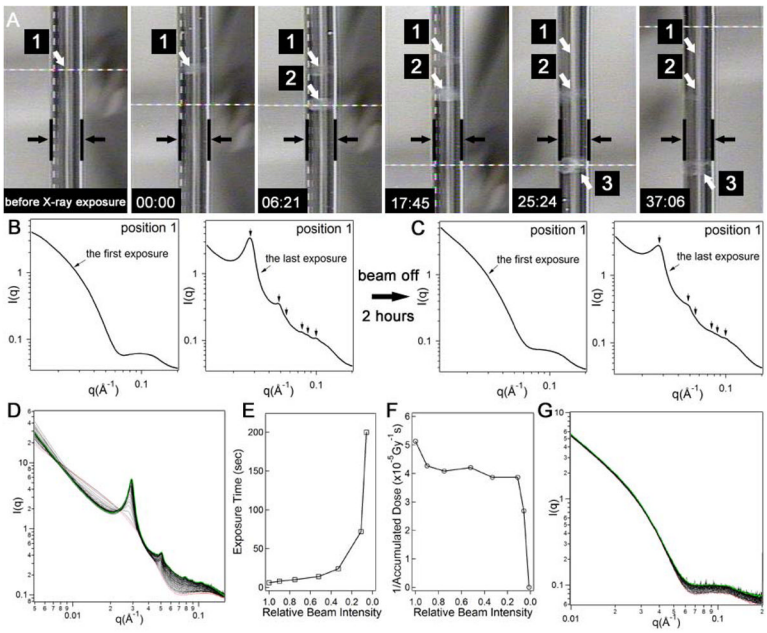

Figure 3.

Reversible crystallization of filaments triggered by X-ray irradiation and the effects of the X-ray beam attenuation and photon energy. **(A)** A series of sequential photographs of the quartz capillary loaded with sample reveal the optical appearance changes before and after X-ray irradiation. The parallel black lines in the photographs demarcate the edges of the capillary and the white arrows point to the three spots (labeled as **1**, **2**, and **3**) irradiated with X-rays for 200 s (the cylindrical shape visible within the space of the capillary is just an artifact of the photograph). From left to right, the first photograph corresponds to a sample-loaded capillary before X-ray irradiation and the second one shows opacity in spot **1** after 200 s irradiation (indicated as time 00:00 in the lower left hand corner of the photograph). Subsequent photographs from left to right reveal changes in the appearance of spots **1**, **2** and **3** after the elapsed times indicated in the left hand corner of the photographs (minutes:seconds). The opacity in the irradiated spots dimmed eventually in the absence of the X-ray beam; **(B)** one-dimensional scattering profile after the first X-ray exposure of 4 seconds at position **1** and after the last of 49 additional exposures on the same position (all exposures lasted 4 s and the dose rate was 4806 Gy/second); **(C)** after a waiting period of two hours with the beam off, the experiment in (**B)** was repeated on position **1** and similar scattering profiles were obtained; **(D)** 50 consecutive scattering profiles from 1 wt % aqueous solution with a photon energy of 9 keV (exposure time = 2 seconds; photon flux = 2.2×10^{11} photons/second; beam size = 0.37 mm × 0.31 mm; dose rate: 1037 Gy/second). The first and last spectra are colored red and green, respectively; **(E)** plot of accumulated X-ray exposure time required for observation of the principal Bragg peak as a function of relative beam intensity; **(F)** plot of the reciprocal of accumulated X-ray dose as a function of relative beam intensity; **(G)** the first 50 consecutive scattering profiles from 1 wt % aqueous solution (exposure time = 16 seconds; photon flux = 1.5×10^{10} photons/second; beam size = 0.37 mm × 0.31 mm; dose rate = 39.22 Gy/second).

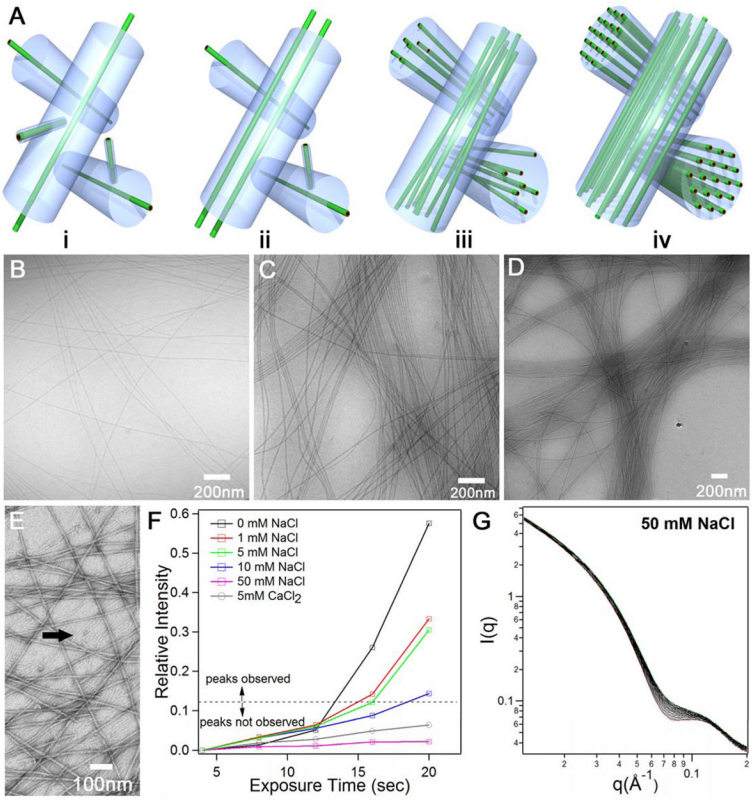

Figure 4.

(A) Schematic illustration of the proposed templating model for filament bundle formation during self-assembly. **i**, At early stages of self-assembly, interlocking of long filaments leads to the formation of a channel around each one of them. The long filament has many degrees of freedom within its channel, but cannot leave it or allow others enter its space. The volume of this imaginary channel should be determined mostly by the bulk density of long filaments; **ii**, newly formed long filaments from smaller ones and from monomer are confined to grow within these channels; **iii**, further growth causes the formation of bundles of aligned long filaments; **iv**, at high concentrations hexagonally ordered filaments are spontaneously formed as a result of repulsive electrostatic forces and network confinement; **(B)** cryo-TEM image of filament bundles in 0.5 wt % solutions, 1 wt % solutions (**C**), and 2 wt % solutions (**D**); (**E**) negatively stained TEM image of very early stages of self-assembly revealing clearly the presence of small aggregates (marked with black arrow) coexisting with loosely packed long filaments at 0.1 wt % (this image offers support for the templating mechanism for bundle formation explained in (**A**)); **(F)** the effect of added salts on X-ray triggered crystallization of filaments: plot of the intensity of the primary Bragg peak as a function of exposure time to X-rays in 1 wt % solutions, when the intensity plotted is below the dotted line the Bragg peak was not observed; (**G**) 50 X-ray scattering profiles corresponding to a 1 wt % solution containing 50 mM concentration of NaCl obtained sequentially after 50 exposures of 4 s each to the X-ray beam (dose rate: 4806 Gy/second).